Anomalous correlation between quantum efficiency and transverse momentum spread in semiconductor cathode photoemission

Peng-Wei Huang,[1,2,3,*] Houjun Qian,[1,†] Ye Chen,[1] Matthias Gross,[1] Igor Isaev,[1] Christian Koschitzki,[1] Mikhail Krasilnikov,[1] Shankar Lal,[1] Sven Lederer,[4] Xiangkun Li,[1] Osip Lishilin,[1] David Melkumyan,[1] Laura Monaco,[5] Paolo Michelato,[5] Raffael Niemczyk,[1] Anne Oppelt,[1] Daniele Sertore,[5] Hamed Shaker,[1] Guan Shu,[1] Frank Stephan,[1] Chuanxiang Tang,[2,3] and Grygorii Vashchenko[1]

[1]*Deutsches Elektronen-Synchrotron DESY, Platanenallee 6, 15738 Zeuthen, Germany*
[2]*Department of Engineering Physics, Tsinghua University, Beijing 100084, China*
[3]*Key Laboratory of Particle and Radiation Imaging, Tsinghua University, Ministry of Education, Beijing 100084, China*
[4]*Deutsches Elektronen-Synchrotron DESY, Notkestrasse 85, 22607, Hamburg, Germany*
[5]*Istituto Nazionale di Fisica Nucleare, Milano–LASA, Segrate, I-20090, Italy*

(Received 11 February 2022; accepted 26 April 2022; published 12 May 2022)

The next generation of accelerator based scientific facilities, such as the megahertz repetition rate free electron laser and electron-ion collider, relies on photoelectron sources of high peak and high average brightness. Therefore, photocathodes with both low transverse momentum spread (TMS) and high quantum efficiency (QE) are required. The conventional positive correlation between QE and TMS leads to a tradeoff between peak and average brightness. In this study, a negative correlation between QE and TMS is experimentally observed for the first time on a semiconductor photocathode (Cs_2Te). Two models are proposed to explain such an anomalous correlation. One model considers the junction between the semiconductor cathode and the metal substrate in the case of slightly excessive cesium deposition, and the other model considers different Cs-Te composites. Our studies inspire a new way to break the conventional correlation between QE and TMS, and open a new perspective to advance the beam brightness frontiers.

DOI: 10.1103/PhysRevAccelBeams.25.053401

I. INTRODUCTION

High electron beam brightness, i.e. high phase space density, is vital for the performances of many accelerator based scientific facilities, such as the brilliance of light sources based on linac and synchrotron, transverse coherence and spatial resolution of electron microscope, luminosity of colliders, etc. [1–4]. According to Liouville's theorem, the maximum beam brightness is determined by the electron source for a linac with a defined energy. The phase space area of the electron beam at the cathode, i.e. the intrinsic emittance, is a product of the rms beam size σ_c and the rms normalized transverse momentum spread (TMS) σ_p,

$$\varepsilon_{\text{in}} = \sigma_c \frac{\sigma_p}{m_0 c}, \tag{1}$$

where m_0 is the electron's rest mass and c is the speed of light. Compared to thermionic emission and field emission, photoemission electron sources based on ultrafast (femtosecond to picosecond) lasers deliver high brightness in both transverse and longitudinal phase space, and have been widely used to drive free electron lasers and ultrafast electron diffraction facilities since the 1980s [5,6]. While the cathode laser spot size is limited either by optical focusing or by emission saturation under space charge effect [7,8], the photoemission TMS is the key parameter under intense R&D to meet the ever-increasing demand on beam brightness [9,10]. According to the traditional bulk photoemission theories, TMS is positively correlated to quantum efficiency (QE) and both are proportional to the difference between photon energy and emission threshold [9,11]. Although the surface photoemission of some types of metals has shown the sign of negative correlation between QE and TMS [12,13], the semiconductor photocathode is dominated by bulk photoemission when the driven photon energy is beyond the emission threshold.

*hpw17@mails.tsinghua.edu.cn
†houjun.qian@desy.de

To achieve ultralow TMS, QE is usually sacrificed, for example by lowering the incident photon energy [14,15]. This strategy works well for low repetition rate (<1 kHz) and low average current (<1 μA) facilities because of the high pulse energy of sub-kHz class photocathode lasers [9].

Based on the advances of continuous wave (cw) superconducting linac [16,17], the next generation of x-ray free electron lasers (FELs) and ultrafast electron microscopes are under design and construction to reach both high peak and high average brightness [18–21]. The beam repetition rate will be increased by 3 to 4 orders of magnitude to reach a higher average current (<1 mA) [22]. Since the pulse energy is much lower for MHz class lasers and similar bunch charge is still required, high QE photocathodes ($>0.5\%$) are preferred, and up to date semiconductors are very practical choices [9]. The headroom of laser energy and QE will be even more limited for the facilities which require an electron beam of even higher average current (up to ~100 mA), such as the energy recovery linac based light source and electron cooling for the electron ion collider [4,23]. Usually the green cathode is applied instead of the UV cathode due to the advantage of both high QE and high conversion efficiency for the green laser [9]. Besides, current x-ray FEL designs based on the cw linac expect a lower beam energy than the pulse linac to reduce the superconducting radio frequency (SRF) operation cost [18,19], so a higher beam peak brightness from the electron source is preferred to improve lasing at the shortest wavelength [24]. Therefore, a comprehensive improvement of both QE and TMS for photocathodes will benefit a wide scientific community, which poses a great challenge for the photocathode R&D.

The challenge is to improve both QE and TMS results from their positive correlation. One should notice that the derivation of the positive correlation is based on the traditional bulk photoemission theory. The theory does not include surface photoemission, where the special surface band dispersion and the absence of the scatterings lead to different performances from the bulk photoemission. The participation of surface states is confirmed to improve both QE and TMS within a limited range of incident photon energy for a single crystal Ag cathode [12]. Besides, the surface plasmon assisted photoemission can enhance the QE by a factor of 10 without degrading TMS on the Mg cathode [13]. Both are metal cathodes, for which the QE of bulk photoemission is low ($10^{-5} \sim 10^{-4}$). In contrast, the semiconductor cathode has a much higher QE from bulk photoemission and the surface photoemission is negligible. The traditional theory also neglects the effects of the interaction between the semiconductors and the substrates. Measurements during Cs_2Te cathode deposition on the Mo substrate show that both QE and emission threshold energy decrease after the final QE peak [25], which indicates that the TMS increases accompanied with QE decrease, a negative correlation of QE and TMS. Since the Cs_2Te deposition process is not perfectly uniform in the cathode area, there is naturally a nonuniform spatial distribution for both QE and TMS, which can be used to make a correlation study. The QE map is a routine measurement to most photoinjectors, but a complete TMS map has never been achieved [26].

In this paper, a correlation study of QE and TMS is presented on semiconductor cathodes (Cs_2Te). We first introduce a cathode TMS mapping method based on a single shot cathode TMS imaging technique [27]. We then present the QE map and the TMS map of the Cs_2Te cathode, and negative correlations between QE and TMS are observed. Finally, two models are presented to explain such an anomalous correlation.

II. METHOD

The experiment is done at the Photo Injector Test Facility at DESY, Zeuthen site (PITZ). The schematic of the experimental setup is presented in Fig. 1. In our experiments, the electrons' mean momentum at the gun exit was 5.8 MeV/c. The corresponding emission electric field was roughly 41 MV/m. The laser wavelength was 257 nm and the beam was transversely uniform with a ~6 ps FWHM duration. Laser position on the cathode was steered by motorized mirrors. Beam charge was measured from a downstream Faraday cup, and laser energy was monitored online by splitting a fraction of the laser to the energy meter. Beam size was measured with a lutetium yttrium orthosilicate (LYSO) screen [28] and a CCD camera. For QE mapping, the solenoid was tuned to focus the electron beam to the Faraday cup. For TMS mapping, the solenoid was tuned to make the LYSO screen at the back focal plane of the combined lens system formed by the gun rf field and the solenoid magnetic field, so the beam size measured at the LYSO screen is proportional to the TMS at the cathode [27].

Almost all measurement points in a TMS map are off axis in the rf gun, and a rf kick will induce an emittance growth, leading to an overestimation of the TMS. The rf induced emittance growth for the off axis beam in the rf gun is derived as follows [29]:

$$\varepsilon_{RF} \approx \frac{eE_z}{2m_0c^2}\sigma_x\sigma_\phi \cos\phi_f\sqrt{x_0^2+\sigma_x^2}, \tag{2}$$

where σ_ϕ and σ_x are the rms bunch length in terms of rf phase and the rms beam size at the gun exit, respectively.

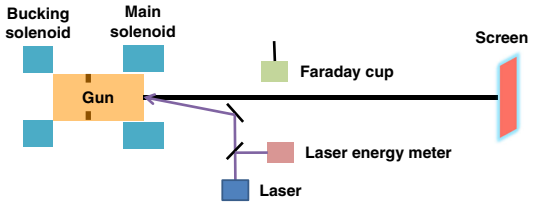

FIG. 1. Schematic of the experimental setup.

e is the elementary charge and E_z is the peak field on axis. ϕ_f refers to the rf synchronous phase of the beam center at the gun exit and it is different from the beam phase at the cathode due to phase slippage. x_0 denotes the mean horizontal offset relative to gun axis on the cathode. As an example, the Cs_2Te film on the plug used in the PITZ gun has a diameter of 5 mm. With a rms laser spot size of 0.125 mm, the rf induced emittance growth will lead to a 30% overestimation of the intrinsic TMS at the cathode edge ($r = 2.5$ mm) with the mentioned gun exit energy under the maximum acceleration phase. Therefore, the rf induced emittance growth has to be reduced, especially for low TMS cathodes. According to Eq. (2), the rf induced emittance for an off axis beam can be reduced by a lower electric field, smaller beam size and shorter bunch length, but such measurement will require a lower bunch charge due to the space charge effect, and make the beam size measurement more vulnerable to signal to noise ratio. In our experiment, the rf emittance is minimized by tuning the ϕ_f to be 90 degrees, which increases the bunch charge to 100 fC with the above laser parameters.

Such a special rf gun phase is easily found by simulations, and here we also show how to determine it experimentally. The TMS imaging is carried out versus different rf phases for one off axis position of the cathode, and a minimum beam size is expected when the rf induced emittance growth is minimized. The measurements and the simulations are presented in Fig. 2(a). The smallest beam size is achieved at 8.8 degrees with respect to the maximum mean momentum gain (MMMG) phase, which is a reference phase determined by electron beam energy measurement. Compared to the TMS imaging at the cathode center where rf emittance is negligible, the beam sizes of the off axis case clearly overestimate the TMS except gun phase of MMMG + 8.8 degrees. Another evidence of the rf emittance minimization with the special gun phase is shown in Fig. 2(b). With the off axis rf kick, the rf emittance growth is not equally distributed between the x and the y plane after Larmor rotation in the gun solenoid, so the beam shows asymmetry when rf emittance growth is significant, e.g. at MMMG phase. The beam symmetry is restored at phase MMMG + 8.8 degrees due to the mitigation of rf emittance growth. Although the above calculation is specified for the PITZ gun, the method is generally applicable for other types of electron guns, where the special phase may differ due to the rf frequency, half cell length and number of cells.

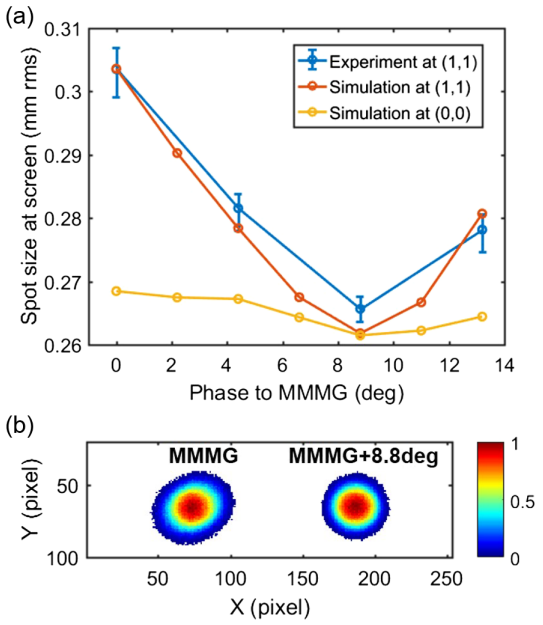

FIG. 2. (a) Minimization of rf induced emittance growth for the off axis beam by a special rf phase. The off axis laser position is (1,1) relative to the cathode center with units of millimeter. (b) Off axis electron beam images measured at gun phases of MMMG and MMMG + 8.8 degrees.

III. RESULTS AND DISCUSSION

In total, four different Cs_2Te cathodes have been measured in this experiment. Three of them are fresh cathodes with different Te thicknesses [30,31], and they are numbered as #678.1, #672.1 and #676.1, whose Te thicknesses are 15, 10 and 5 nm, respectively. The fourth one is a used cathode with 10 nm Te thickness, numbered as #661.1. An example of the QE map and the TMS map of cathode #678.1 is presented in Fig. 3, and the correlations between QE and TMS of the four cathodes are displayed in Fig. 4. A negative correlation, i.e. higher QE positions have lower TMS, is clearly observed for all four cathodes, which breaks the traditional positive correlation between QE and TMS. The above measurements were taken at an emission electric field of 41 MV/m. An additional measurement was made at a lower electric field of 16 MV/m on the used cathode #661.1 and a similar negative correlation was still observed, though the QE and TMS are both lower than those at 41 MV/m. As a comparison, the dependence of TMS on the emission field is much less for the three fresh cathodes [30]. This indicates the surface roughness of the used cathode is much worse than the fresh cathodes [32–34], but surface roughness is probably not responsible for such a negative correlation since it is observed for cathodes of both high and low surface roughness.

The cathodes are produced with a sequential deposition recipe developed by the LASA group at INFN Milano [25]. The Te element is deposited first and after the Te thin film reaches the desired thickness, like 10 nm, the Cs deposition begins and is controlled by the QE monitoring. The Cs deposition is terminated after the final QE peak [25]. According to the Auger depth profile studies [35], the Cs_2Te film is roughly 30 nm thick with a constant Cs/Te ratio slightly above 2 due to the excess cesium. The evaporation thickness of the three fresh cathodes (#678.1, #672.1 and #676.1) are well documented, listed

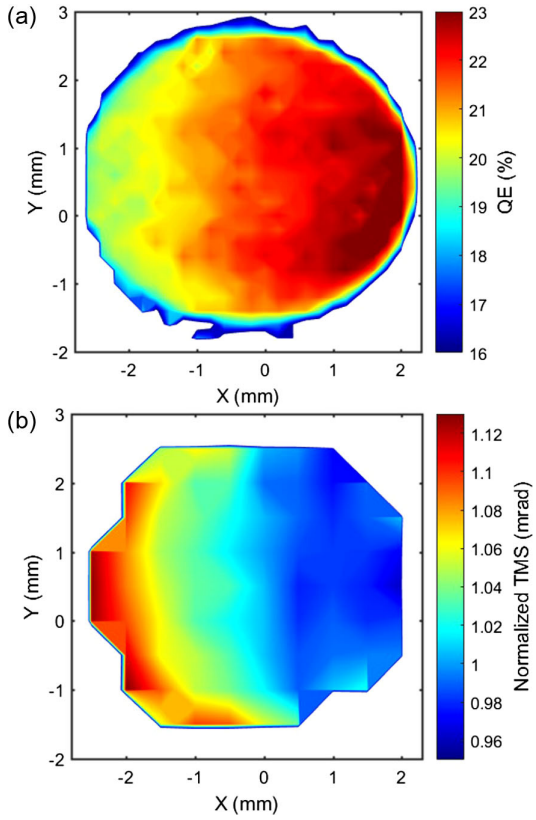

FIG. 3. QE map (a) and TMS map (b) of the Cs_2Te cathode #678.1. The QE map is measured with the laser diameter of 0.25 mm and the step size of 0.2 mm. The TMS map is measured with laser diameter of 0.5 mm and the step size of 0.5 mm.

in Table I, and the details of the old cathode (#661.1) are similar to #672.1. A previous study of Cs_2Te cathode deposition on a Si substrate by x-ray diffraction shows the high QE (~19% at 266 nm) cathode is dominated by the Cs_2Te phase, while a lower QE (~8%) cathode is dominated by two Cs-Te phases, Cs_2Te and Cs_2Te_3 [36]. Since our fresh cathodes have high QE above 20%, it is reasonable to believe our cathodes are dominated by the Cs_2Te phase. Compared to the QE peak, we found that the

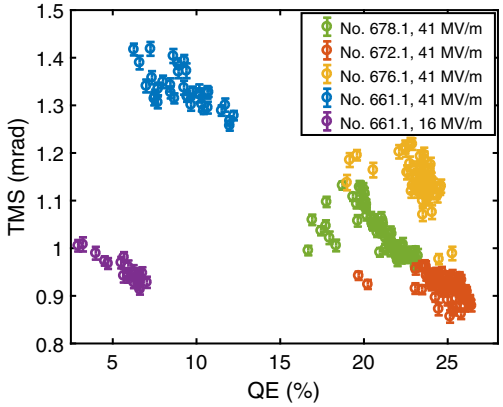

FIG. 4. The correlation of TMS and QE of four Cs_2Te cathodes.

TABLE I. The evaporation thickness of the three fresh cathodes.

Cathode	Te evaporation thickness (nm)	Cs thickness for Cs QE peak (nm)	Cs total evaporation thickness (nm)
#678.1	15.1	90.71	92.22
#672.1	9.8	61.87	63.29
#676.1	5.1	33.03	33.88

relative excess Cs evaporated of the three fresh cathodes are 1.67%, 2.3% and 2.57%, respectively. Therefore, the cathode is anion vacancy type or cation interstitially type, equivalent to n-type semiconductor [37]. The cathodes used in the experiments are deposited on the Mo plug, which forms a Schottky barrier in the metal-semiconductor junction, leading to the band bending in the semiconductor, as shown in Fig. 5. Due to the low excess Cs deposition, the charge carrier density in Cs_2Te is expected to be not significantly high, on the 10^{18} cm^{-3} level, so the depletion region of the junction will cover the whole Cs_2Te film thickness (~30 nm). In the junction, ion scattering is much stronger due to the lack of electron screening. The high ion density induces large photoelectron loss, which is confirmed experimentally on GaN [38]. The continuous drop of emission threshold after the final QE peak in the cathode deposition experiments [25] could be caused by the band bending in the depletion region. In contrast to the drop of emission threshold, a QE reduction may result from the electron scattering loss with ions. Consequently, a lower QE and a higher TMS will be obtained with excess cesium deposition after the final QE peak. The inhomogeneity of the excess Cs over the whole cathode is naturally formed during the deposition. Therefore, our observations of the negative correlation between QE and TMS within each cathode might be attributed to the variation of the local excess Cs density in the mapping area.

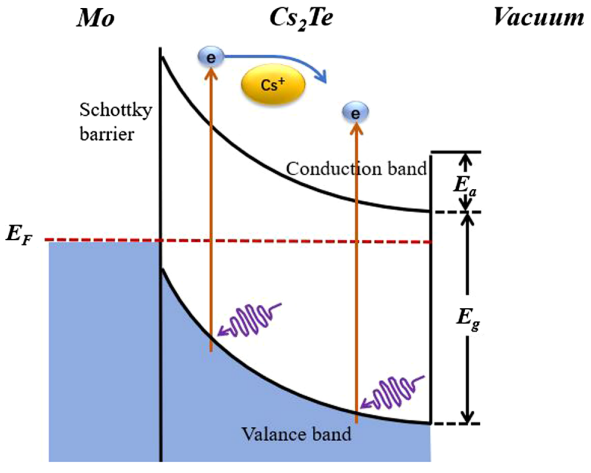

FIG. 5. The schematic of the Schottky barrier model in the junction between Cs_2Te and Mo substrate.

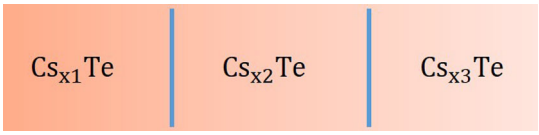

FIG. 6. The schematic of the multiple Cs-Te phases model. The x_1, x_2 and x_3 in the schematic refer to the chemical ratio. The cathode sample contains several Cs-Te phases, assuming from $Cs_{x1}Te$ to $Cs_{x3}Te$ the QE increases and the TMS decreases. This can also lead to the negative correlation between QE map and TMS map.

Another model to explain the negative correlation is attributed to multiple Cs-Te phases in the cathode, as shown in Fig. 6, which was observed for sequential deposited cathodes, although the high QE ($>20\%$) of the three fresh cathodes indicates a dominant Cs_2Te phase [36]. If the cathode includes a significant amount of other Cs-Te composites, such as Cs_3Te_2, CsTe, Cs_2Te_3, Cs_2Te_5, etc. [39], and these Cs-Te phases have lower QE but higher TMS, which need further experimental verification, then the variation of the other Cs-Te phases relative to the Cs_2Te phase can also lead to a negative correlation between QE and TMS. Since the Cs/Te ratios of the other composites are all below 2, such a model will lead to a Cs/Te ratio below 2, which is not consistent with the previous measurement of the Cs/Te ratio above 2 [35]. Therefore, more studies are needed to clarify which model fits the real cathode better.

IV. SUMMARY

In this study, a negative correlation between QE and TMS is experimentally observed for four thin film (30 nm) semiconductor photocathodes (Cs_2Te). Such a negative correlation is consistent with the reduction of both QE and emission threshold during the excess cesium deposition [25]. One photoemission model considering the junction between the cathode and the substrate is proposed to explain such a negative correlation. When excess cesium deposition starts after the QE peak, a n-type Schottky barrier is formed, and the thin cathode is inside the depletion region. Both the band bending and the ion scattering are enhanced with increased excess cesium density, leading to a lower QE and higher TMS, i.e. a negative correlation. Another explanation of the negative correlation is based on the mixture of different phases of Cs-Te composites, provided that the other phases of Cs-Te have a lower QE but higher TMS than the Cs_2Te phase. Although the clarification of these two models still needs further experimental studies, it still inspires us to improve the semiconductor cathode in both QE and TMS, e.g. by reducing the band bending near the cathode substrate [40,41], or by codeposition to achieve a single phase dominated photocathode [36], which will push the electron source brightness frontier and benefit the next generation of scientific facilities demanding even higher peak and average beam brightness [4,18,20].

[1] M. Yabashi and H. Tanaka, Nat. Photonics **11**, 12 (2017).
[2] S. Weathersby, G. Brown, M. Centurion, T. Chase, R. Coffee, J. Corbett, J. Eichner, J. Frisch, A. Fry, M. Gühr *et al.*, Rev. Sci. Instrum. **86**, 073702 (2015).
[3] R. Li and P. Musumeci, Phys. Rev. Applied **2**, 024003 (2014).
[4] A. Accardi, J. Albacete, M. Anselmino, N. Armesto, E. Aschenauer, A. Bacchetta, D. Boer, W. Brooks, T. Burton, N.-B. Chang *et al.*, Eur. Phys. J. A **52**, 268 (2016).
[5] G. Mourou and S. Williamson, Appl. Phys. Lett. **41**, 44 (1982).
[6] R. Sheffield, E. Gray, and J. Fraser, Nucl. Instrum. Methods Phys. Res., Sect. A **272**, 222 (1988).
[7] I. V. Bazarov, B. M. Dunham, and C. K. Sinclair, Phys. Rev. Lett. **102**, 104801 (2009).
[8] D. Filippetto, P. Musumeci, M. Zolotorev, and G. Stupakov, Phys. Rev. ST Accel. Beams **17**, 024201 (2014).
[9] D. Dowell, I. Bazarov, B. Dunham, K. Harkay, C. Hernandez-Garcia, R. Legg, H. Padmore, T. Rao, J. Smedley, and W. Wan, Nucl. Instrum. Methods Phys. Res., Sect. A **622**, 685 (2010).
[10] P. Musumeci, J. G. Navarro, J. Rosenzweig, L. Cultrera, I. Bazarov, J. Maxson, S. Karkare, and H. Padmore, Nucl. Instrum. Methods Phys. Res., Sect. A **907**, 209 (2018).
[11] D. H. Dowell and J. F. Schmerge, Phys. Rev. ST Accel. Beams **12**, 074201 (2009).
[12] S. Karkare, J. Feng, X. Chen, W. Wan, F. J. Palomares, T.-C. Chiang, and H. A. Padmore, Phys. Rev. Lett. **118**, 164802 (2017).
[13] H. Qian, J. Murphy, Y. Shen, C. Tang, and X. Wang, Appl. Phys. Lett. **97**, 253504 (2010).
[14] C. Hauri, R. Ganter, F. Le Pimpec, A. Trisorio, C. Ruchert, and H. Braun, Phys. Rev. Lett. **104**, 234802 (2010).
[15] J. Maxson, L. Cultrera, C. Gulliford, and I. Bazarov, Appl. Phys. Lett. **106**, 234102 (2015).
[16] A. Grassellino, A. Romanenko, D. Sergatskov, O. Melnychuk, Y. Trenikhina, A. Crawford, A. Rowe, M. Wong, T. Khabiboulline, and F. Barkov, Supercond. Sci. Technol. **26**, 102001 (2013).
[17] A. Grassellino, A. Romanenko, Y. Trenikhina, M. Checchin, M. Martinello, O. Melnychuk, S. Chandrasekaran, D. Sergatskov, S. Posen, A. Crawford *et al.*, Supercond. Sci. Technol. **30**, 094004 (2017).
[18] J. Stohr, Technical Report No. SLAC-R-978, SLAC National Accelerator Laboratory, Menlo Park, CA, 2011.
[19] Z. Zhao, D. Wang, Z. Yang, and L. Yin, in *Proceedings of the International Free Electron Laser Conference (FEL'17), Santa Fe, NM, 2017* (JACoW, Geneva, Switzerland, 2018), No. 38, pp. 182–184.
[20] W. Decking, S. Abeghyan, P. Abramian, A. Abramsky, A. Aguirre, C. Albrecht, P. Alou, M. Altarelli, P. Altmann, K. Amyan *et al.*, Nat. Photonics **14**, 391 (2020).
[21] D. Filippetto and H. Qian, J. Phys. B **49**, 104003 (2016).
[22] D. Filippetto, H. Qian, and F. Sannibale, Appl. Phys. Lett. **107**, 042104 (2015).
[23] D. H. Bilderback, J. D. Brock, D. S. Dale, K. D. Finkelstein, M. A. Pfeifer, and S. M. Gruner, New J. Phys. **12**, 035011 (2010).
[24] T. Raubenheimer, in *Proceedings of the 60th ICFA Advanced Beam Dynamics Workshop (FLS'18), Shanghai,*

China, 2018 (JACoW Publishing, Geneva, Switzerland, 2018), No. 60, pp. 6–11.

[25] L. Monaco, P. Michelato, D. Sertore, C. Pagani, and M. Songini, in *Proceedings of the International Particle Accelerator Conference 2010, Kyoto, Japan* (JACoW Publishing, Geneva, Switzerland, 2010), pp. 1719–1721, https://accelconf.web.cern.ch/IPAC10/papers/tupec006.pdf.

[26] L. Zheng, J. Shao, E. E. Wisniewski, J. G. Power, Y. Du, W. Liu, C. E. Whiteford, M. Conde, S. Doran, C. Jing *et al.*, Phys. Rev. Accel. Beams **23**, 052801 (2020).

[27] P.-W. Huang, H. Qian, Y. Chen, D. Filippetto, M. Gross, I. Isaev, C. Koschitzki, M. Krasilnikov, S. Lal, X. Li *et al.*, Phys. Rev. Accel. Beams **23**, 043401 (2020).

[28] R. Niemczyk, P. Boonpornprasert, Y. Chen, J. Good, M. Groß, H. Huck, I. Isaev, D. Kalantaryan, C. Koschitzki, M. Krasilnikov *et al.*, in the *7th International Beam Instrumentation Conference (IBIC'18), Shanghai, China, 2018* (JACOW Publishing, Geneva, Switzerland, 2019), pp. 438–440.

[29] K. Floettmann, Phys. Rev. ST Accel. Beams **18**, 064801 (2015).

[30] P. Huang *et al.*, in *Proceedings of FEL'19* (JACoW Publishing, Geneva, Switzerland, 2019), No. 39, pp. 473–476.

[31] L. Monaco, G. G. Rocco, P. Michelato, C. Pagani, and D. Sertore, in *Proceedings of FEL'19* (Ref. [30]), pp. 297–300.

[32] H. Qian, C. Li, Y. Du, L. Yan, J. Hua, W. Huang, and C. Tang, Phys. Rev. ST Accel. Beams **15**, 040102 (2012).

[33] Z. Zhang and C. Tang, Phys. Rev. ST Accel. Beams **18**, 053401 (2015).

[34] G. Gevorkyan, S. Karkare, S. Emamian, I. Bazarov, and H. Padmore, Phys. Rev. Accel. Beams **21**, 093401 (2018).

[35] A. Di Bona, F. Sabary, S. Valeri, P. Michelato, D. Sertore, and G. Suberlucq, J. Appl. Phys. **80**, 3024 (1996).

[36] M. Gaowei, J. Sinsheimer, D. Strom, J. Xie, J. Cen, J. Walsh, E. Muller, and J. Smedley, Phys. Rev. Accel. Beams **22**, 073401 (2019).

[37] J.-L. Zhang and G.-Y. Hong, in *Modern Inorganic Synthetic Chemistry (Second Edition)*, edited by R. Xu and Y. Xu (Elsevier, Amsterdam, 2017), pp. 329–354.

[38] X. Wang, B. Chang, L. Ren, and P. Gao, Appl. Phys. Lett. **98**, 082109 (2011).

[39] G. Prins and E. Cordfunke, J. Less-Common Met. **104**, L1 (1984).

[40] R. T. Tung, Appl. Phys. Rev. **1**, 011304 (2014).

[41] K.-E. Byun, H.-J. Chung, J. Lee, H. Yang, H. J. Song, J. Heo, D. H. Seo, S. Park, S. W. Hwang, I. Yoo *et al.*, Nano Lett. **13**, 4001 (2013).